PROCEEDINGS OF SCIENCE

Cosmic Ray Composition at IceTop and IceCube, using Graph Neural Networks

The IceCube Collaboration

(a complete list of authors can be found at the end of the proceedings)

E-mail: paras.koundal@icecube.wisc.edu

The IceCube Neutrino Observatory, along with its surface array IceTop, is a unique instrument for identifying the elemental composition of cosmic rays around the transition region between Galactic and extragalactic origin of cosmic rays. It can thus provide valuable insights into identifying astrophysical sources of high-energy particles. This work reports the preliminary cosmic-ray composition estimate for air showers detected in IceCube. The analysis is performed by an integrated use of a graph neural network (GNN) based approach, along with reconstructed air-shower features. The GNN uses the detector-hits of air showers recorded at IceTop and IceCube, mapped as a graph. The reconstructed features capture multiple aspects of air-shower physics. The implementation of the GNN based approach also provides the flexibility and facilitates the potential incorporation of planned detector extensions in the future.

Corresponding authors: Paras Koundal[1]*

[1] *Institute for Astroparticle Physics, Karlsruhe Institute of Technology, Germany*

* Presenter

The 38th International Cosmic Ray Conference (ICRC2023)
26 July – 3 August, 2023
Nagoya, Japan

PoS(ICRC2023)334

1. Introduction

Cosmic Rays (CRs) are a useful probe to understand astrophysical sources. The IceCube Neutrino Observatory, a cubic-kilometer observatory located close to the geographical South Pole, is well suited to study CRs in the transition range between their Galactic and extragalactic origin. In the coincident operation of IceTop (surface component) and IceCube (in-ice component), the observatory serves as a unique three-dimensional detector. In coincident operation, the observatory provides the ability to detect the electromagnetic and GeV as well as TeV muon content of CR-initiated extensive air showers (EASs). This enables detailed CR composition analysis at the IceCube Observatory. A study into the elemental composition of CRs can pave the way to identify their sources, and to improve our understanding of the propagation mechanisms as well as the source dynamics that can accelerate the nuclei to extreme energies.

This work presents the result of CR composition estimation obtained from the analysis of CR-initiated EAS, detected with IceTop and IceCube. In coincident operation, the observatory is sensitive to CRs with energy between $\approx$ 1 PeV to $\approx$ 1 EeV. For composition estimation this work leverages a hybrid approach of utilizing a Graph Neural Network (GNN) to learn hidden correlations in the shower footprint, along with using multiple air-shower observables to capture high-level EAS information. The work presented here utilizes Monte-Carlo (MC) simulations of EASs using CORSIKA [1], in the energy range: $5.0 \leqslant \log_{10}(\mathrm{E/GeV}) \leqslant 9.0$. FLUKA [2] is used as the low-energy hadronic interaction model, while SIBYLL 2.1 [3] is the high-energy hadronic interaction model. In order to test the validity of the method and to estimate composition, a burnsample (10% of data measured in 2012) is used. Because of limited statistics in the burnsample, the results are presented up to an energy of $\log_{10}(\mathrm{E/GeV}) \leqslant 8.0$. The work is an update and improvement of results presented in Ref. [4], and uses the same quality cuts.

2. Composition-Sensitive Observables : Using TeV Muons

Currently at IceCube we can use multiple EAS observables to understand and estimate CR composition. The current work uses the following high-level EAS observables or "Physics Features":

- $\log_{10}(S_{125})$: S_{125} is the signal expectation at a perpendicular distance of 125 m from the shower axis at IceTop. It is expressed in units of Vertical Equivalent Muons, or “VEM”, which corresponds to the signal deposited by a single muon traversing vertically through an entire IceTop tank. $\log_{10}(S_{125})$ is known to be a reliable energy proxy [5].
- Air shower Zenith and Azimuth: Reconstructed using charge and timing information from IceTop hits.
- $\log_{10}(dE/dX_{1500})$: dE/dX_{1500} is the fit value of energy-loss profile at a slant depth of 1500 m in IceCube (details later in this section and in [5]).
- Total Stochastic Energy: Total energy-loss by high-energy stochastic deposits in IceCube (details in [6]).
- Ratio Parameter: Ratio of $\log_{10}(dE/dX_{1500})$ to linear-function of $\log_{10}(S_{125})$.

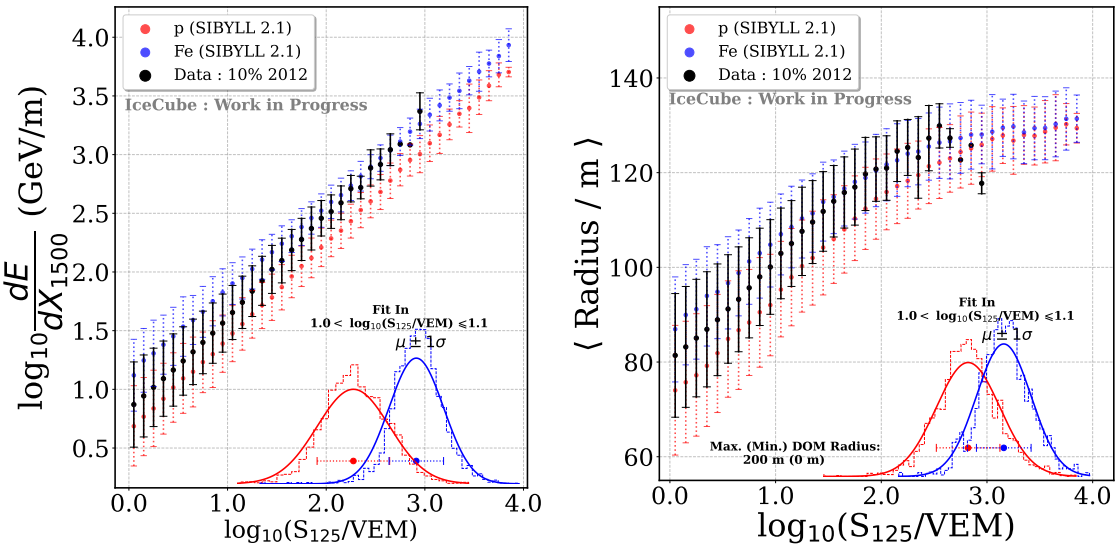

Figure 1: Composition sensitivity of dE/dX_{1500} (*Left*) and R_{mean} (*Right*) as a function of shower size, S_{125}, using SIBYLL 2.1 [3] as the hadronic model and weighted using H4a [10] as the flux-model. The underlying distribution and fits of the parameter for $1 < \log_{10}(S_{125}/\text{VEM}) \leqslant 1.1$ are also depicted in each inset-plot. The distribution from data (10 % of 2012) measured at IceCube is also depicted.

- Mean Radius and Mean Charge: Average lateral spread i.e. *Mean Radius* (R_{mean}) is defined as the mean orthogonal separation of all IceCube hits from the reconstructed track, which are within a maximum distance of 200 m from the reconstructed track. The *Mean Charge* is defined as the average value of the charge deposits, using the same hits which are used to evaluate R_{mean}(details later in this section and in [7]).

The separation power to distinguish between primary mass types varies amongst these EAS observables; in § 3 they will be used together to estimate primary mass using machine learning. This work will elaborate upon the mass sensitivity and separation power of two of these observables, namely $\log_{10}(dE/dX_{1500})$ and R_{mean}. These two observables are related to the multiplicity of TeV muons and their lateral distribution, respectively.

The muon multiplicity in an EAS is considered to be a major observable for composition estimation [8, 9]. The multiplicity of high-energy EAS muons detected with IceCube was found to be correlated with $\log_{10}(dE/dX_{1500})$ [5]. Hence, we can expect mass sensitivity from this observable. Figure 1 (left) presents the value of $\log_{10}(dE/dX_{1500})$, as a function of shower size $\log_{10}(S_{125})$. As expected, dE/dX_{1500} demonstrates a good separation among primary types throughout the full range of energy showcased. Figure 1 (left) also depicts the mean values from the burnsample of data. The burnsample is well bounded between the extreme instances of primary types present in CRs. This, and the effective mass separation capabilities, makes $\log_{10}(dE/dX_{1500})$ a suitable parameter for composition analysis.

At the same energy, iron-initiated EAS are expected to have a wider lateral spread of TeV muons than proton-initiated EAS. This is expected since iron nuclei generally interact earlier in the atmosphere than proton and have a higher muon multiplicity in the considered energy range. This leads to a greater

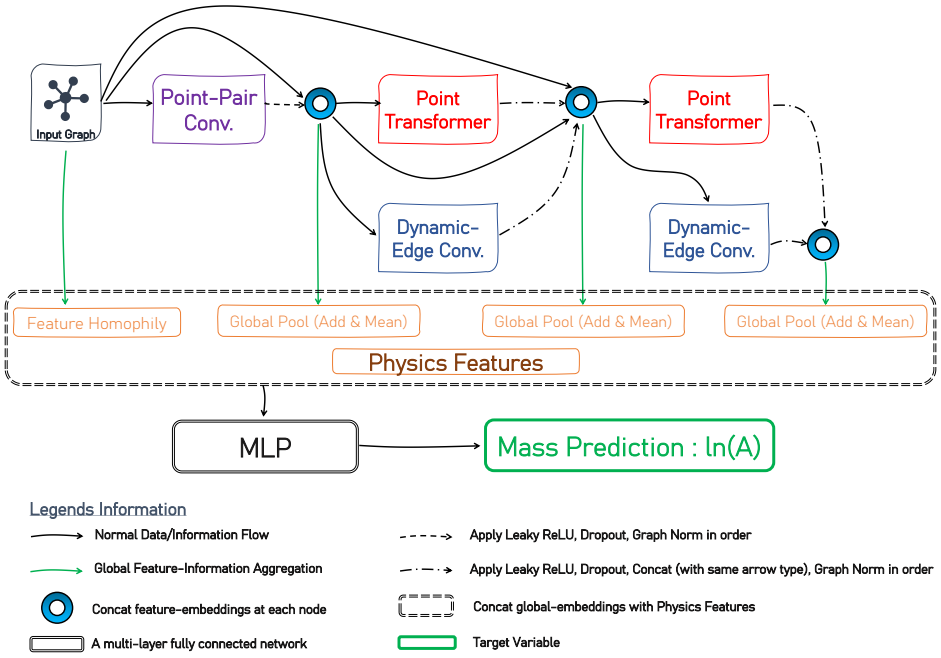

Figure 2: GNN-based architecture utilizing detector hits at IceTop and IceCube ("Input Graph") and EAS observables ("Physics Features"). Further details of the network architecture are provided in [4] and [7].

expectation of muons with larger transverse momenta positioned farther from the shower axis for iron-initiated EAS than proton ones. A measure potentially sensitive to this effect, R_{mean} is evaluated. The mass sensitivity of R_{mean} is depicted in Figure 1 (right). Similarly to dE/dX_{1500}, it is a mass sensitive parameter, and the burnsample data is well contained within expectations from simulations. The separation power of dE/dX_{1500} is however much better than R_{mean}. Improving the separation capabilities of R_{mean} is an ongoing effort.

3. Characterizing Composition : Using Graph Neural Networks

The mass sensitive "Physics Features" listed earlier primarily depend on the deposit of the TeV muons in IceCube. In order to learn more hidden correlation in the shower footprint not captured by the earlier listed observables and improve the primary-type separation capabilities of the analysis, a GNN based approach is utilized to predict a mass proxy (logarithmic mass i.e. ln(A)) for each event.

The architecture of the GNN is shown in Figure 2 and the details of the architecture are provided in [4] and [7]. As a brief summary, the network uses each coincident event, mapped as a graph, as an input for the GNN, labelled "Input Graph" in Figure 2. The hit tanks at IceTop, along with hit DOMs in IceCube, are mapped as nodes of the graph. In order to capture the details of the deposits in the detector, each node has attributes which capture the spatio-temporal and charge hit information in each event. In order to define the node neighborhood (or edges) at each node, the k-nearest neighbor (kNN) algorithm is utilized. Each node is connected to its k nearest neighbors spatially. The exact value of k for each event is based on event size (number of hits) and Ratio Parameter; the formula governing it is presented in [4], with details in [7]. The choice of the architecture as well as the edge-construction allows for a

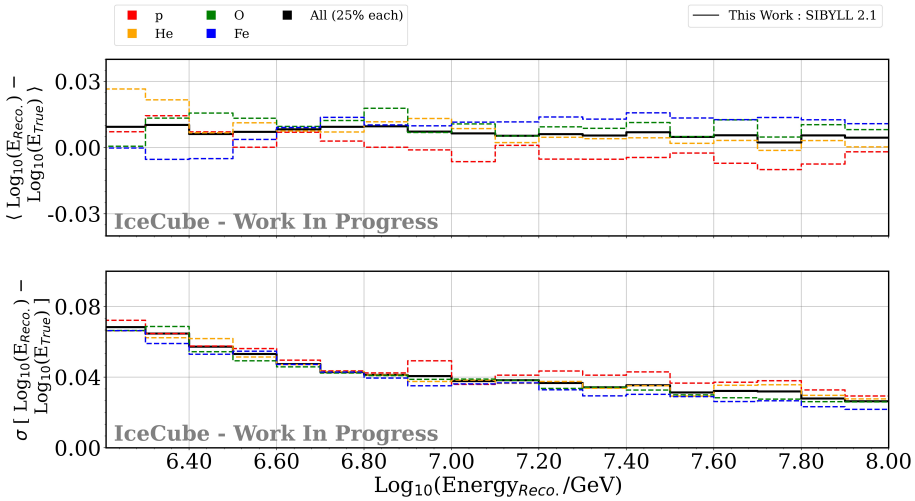

Figure 3: Bias (upper) and resolution (lower) of energy prediction, as a function of reconstructed energy for an equal mixture of all primary types and individual primaries. The energy prediction is obtained using a GBDT, trained on high-level air shower observables.

data efficient training of the network, while also providing improved composition discrimination among the primaries. In order to also benefit from the "Physics Features" listed earlier, the GNN architecture combines them with the global representation learned from each event mapped as a graph. The GNN architecture is trained on an equal mixture of MC simulations of the four primary types (proton = p, Helium = He, Oxygen = O and Iron = Fe). The GNN architecture is trained to predict ln(A) as a mass proxy for each event.

The performance of the GNN architecture is found to be more robust when trained using only a single target variable rather than two (such as mass and energy). Hence, to estimate the primary energy of the events: a Gradient-Boosted Decision Tree (GBDT) is utilized. Several physics features were tested as inputs to the GBDT, and what was found to be most effective was to use all of the GNN's "Physics Features" except for *Mean Charge*. The bias and resolution of energy prediction on the test dataset (a dataset not used during any procedure of training) are shown in Figure 3. Minimal energy bias and improving resolution with increasing energy, are observed.

With a mass proxy obtained from the GNN, and an energy reconstruction from the GBDT, the last step is to determine the fractional contribution of each primary type, using a Template-Fitting approach similar to the previous composition measurement using IceTop and IceCube [5]. Adaptive Kernel Density Estimate (KDE) using the improved Sheather-Jones algorithm [11], is applied to generate templates from different primary types. This process utilizes Monte Carlo simulations from the test dataset. The Template Fitting method can be expressed as finding solutions for:

$$\textbf{Data} = N_p \cdot \mathrm{KDE}_p + N_{He} \cdot \mathrm{KDE}_{He} + N_O \cdot \mathrm{KDE}_O + N_{Fe} \cdot \mathrm{KDE}_{Fe}, \tag{1}$$

where **Data** represents the burnsample distribution in a reconstructed energy bin. $\mathrm{KDE}_{p/He/O/Fe}$ are the template KDEs obtained using the MC simulations. $N_{p/He/O/Fe}$ are the free parameters of the extended likelihood-maximization procedure performed to obtain the reconstructed number of events for each

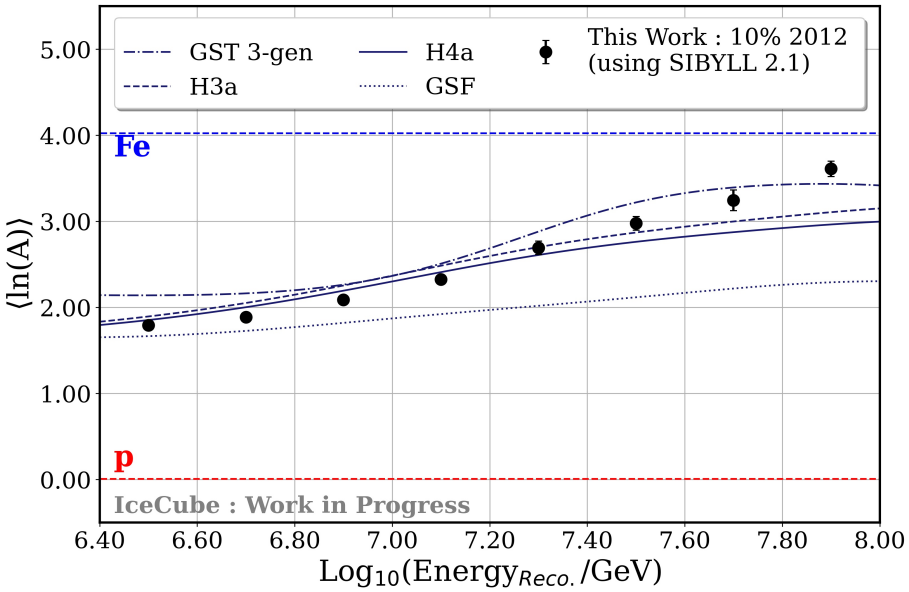

Figure 4: Mean-mass expectation from this work using 10% of data from 2012 as a function of reconstructed energy, obtained using ln(A) predictions from GNN followed by *Template Fitting* procedure. The dashed/dotted lines represent a choice of flux-models among GST 3-gen [13], H3a/H4a [10] and GSF [14]. No systematics are included.

primary type, using *Iminuit* [12]. The contributions are then used to estimate *Mean logarithmic-mass* (i.e. $\langle \ln(A) \rangle$) as a function of reconstructed energy, given by:

$$\langle \ln(A) \rangle = f_p \cdot \ln(A_p) + f_{He} \cdot \ln(A_{He}) + f_O \cdot \ln(A_O) + f_{Fe} \cdot \ln(A_{Fe}). \quad (2)$$

$f_\alpha = N_\alpha/(N_p + N_{He} + N_O + N_{Fe})$ is the fractional contribution from primary type α (= p/He/O/Fe) with logarithmic mass $\ln(A_\alpha)$. Here $\ln(A_p) = 0.007$, $\ln(A_{He}) = 1.386$, $\ln(A_O) = 2.772$ and $\ln(A_{He}) = 4.022$. $\langle \ln(A) \rangle$ obtained from the burnsample is shown in Figure 4. With an increase in energy, the composition shows a transition from a lighter to heavier composition, and is generally compatible with most flux models, for the choice of SIBYLL 2.1 as the hadronic interaction model.

4. Consistency Test

To verify the internal consistency of the derived primary-type fractions and thereby $\langle \ln(A) \rangle$ discussed in §3, a compatibility test is performed. This involves weighting the simulation KDE distributions of the EAS observables mentioned in §2, with fractions obtained from §3 and comparing them with the corresponding EAS observable distributions from the burnsample. The test for $\log_{10}(dE/dX_{1500})$ and R_{mean} is depicted in Figure 5. Generally, a good overlap, for all energy bins, between weighted MC simulation expectation and the burnsample for the two shower observables is seen. It is however important to notice that the overlap is better for R_{mean}, than $\log_{10}(dE/dX_{1500})$.

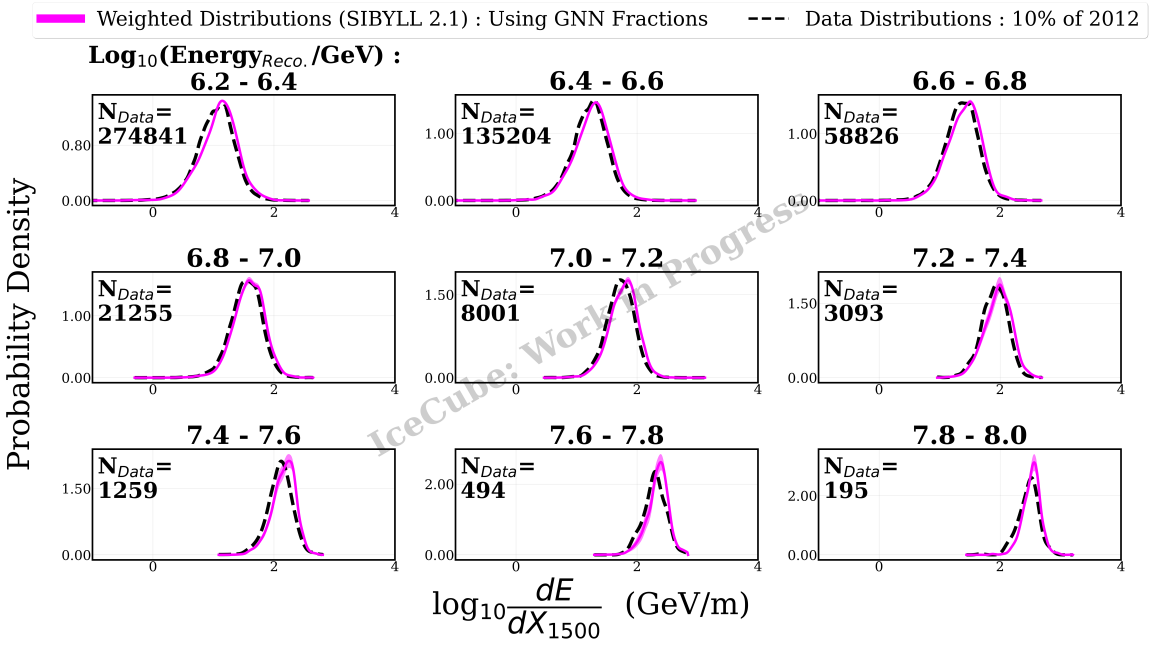

(a) Consistency test for $\log_{10}(dE/dX_{1500})$.

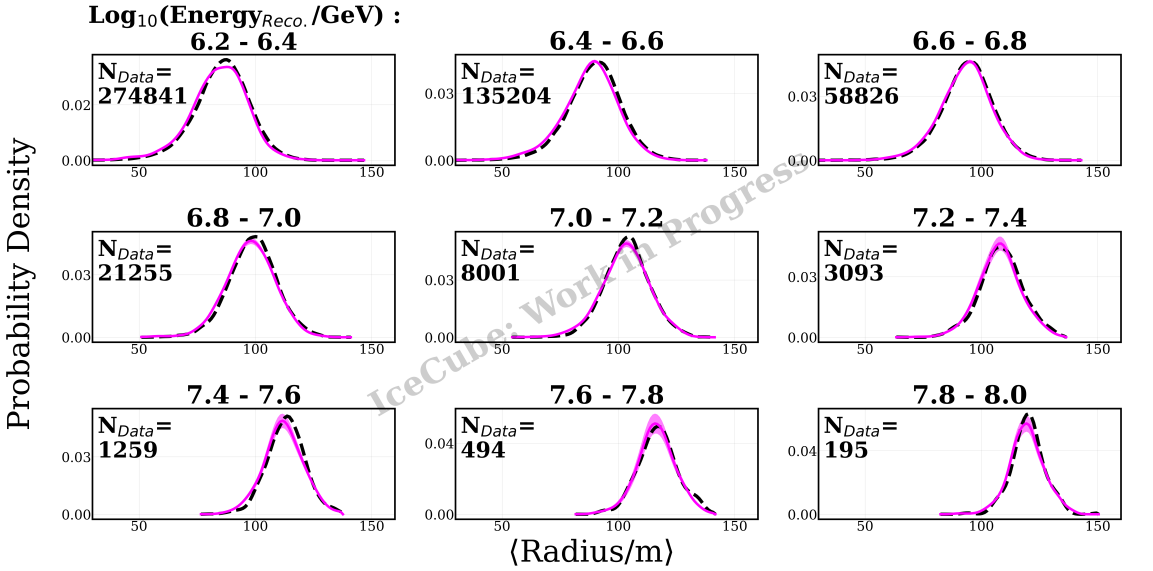

(b) Consistency test for Mean Radius.

Figure 5: Consistency test of composition fractions obtained in this work with distribution from burnsample, in different energy bins. The *Top-panel (a)* depicts the consistency for $\log_{10}(dE/dX_{1500})$ and the *Bottom-panel (b)* for Mean Radius. The magenta-band represents the uncertainty on the weighted MC distribution, obtained by propagating error obtained on the primary type fractions.

5. Conclusions and Outlook

This work presented the *Mean logarithmic-mass* expectation using a burnsample (10% of data measured in 2012), in a coincident operation of IceTop and IceCube. The work used a hybrid approach utilizing multiple EAS observables along with the detector hits, in a GNN-based approach. Analyzed using SIBYLL 2.1, the CR composition indicates a transition from a lighter to heavier composition from $6.4 < \log_{10}(E_{\text{Reco}}/\text{GeV}) \leqslant 8.0$, and in general a good overlap with GST 3-gen [13] and H3a/H4a [10] flux models. A consistency check for the composition expectation indicates a good general agreement between the simulated distributions and with the measurements from burnsample. However, we do see a very slight tension in overlap between the two different EAS observables. We note that a similar composition study has been performed in previous work [5]. Both analyses employ dE/dX_{1500}, but this work uses different and additional inputs for the GNN (not only physics parameters but also IceTop and IceCube hits). The differences between the two analyses can help illuminate inconsistencies in the simulation of EASs. Detailed systematic tests using different hadronic interaction models, detector systematics, and with a dataset larger than the burnsample are required to make a stronger statement/ resolve the tensions seen here.

The analysis also has the possibility to be improved further in the future, by utilizing information from the planned surface enhancement involving scintillation detectors and radio antennas. Augmenting this analysis using measurements from the planned IceCube-Upgrade and the next generation observatory IceCube-Gen2 has the potential to improve the analysis and help extend it beyond the sensitive energy range of the current observatory.

References

[1] D. Heck, J. Knapp, J. Capdevielle, G. Schatz, T. Thouw, *et al. Report FZKA* **6019** no. 11, (1998) .

[2] G. Battistoni, F. Cerutti, A. Fassò, A. Ferrari, S. Muraro, J. Ranft, S. Roesler, and P. R. Sala *AIP Conference Proceedings* **896** no. 1, (03, 2007) 31–49.

[3] E.-J. Ahn, R. Engel, T. K. Gaisser, P. Lipari, and T. Stanev *Phys. Rev. D* **80** (Nov, 2009) 094003.

[4] **IceCube** Collaboration, P. Koundal *PoS* **ECRS** (2023) 085.

[5] **IceCube** Collaboration *Phys. Rev. D* **100** (Oct, 2019) 082002.

[6] **IceCube** Collaboration, P. Koundal, M. Plum, and J. Saffer *PoS* **ICRC** (2021) 323.

[7] P. Koundal, *Elemental Composition of Cosmic Rays : Analysis of IceCube data using Graph Neural Networks (Will be published soon)*. PhD thesis, Karlsruhe Institute of Technology.

[8] K.-H. Kampert and M. Unger *Astroparticle Physics* **35** no. 10, (2012) 660–678.

[9] B. Flaggs, A. Coleman, and F. G. Schröder, "Studying the mass sensitivity of air-shower observables using simulated cosmic rays," 2023. https://arxiv.org/abs/2306.13246.

[10] T. K. Gaisser *Astroparticle Physics* **35** no. 12, (2012) 801–806.

[11] Z. I. Botev, J. F. Grotowski, and D. P. Kroese *The Annals of Statistics* **38** no. 5, (2010) 2916 – 2957.

[12] H. Dembinski, P. Ongmongkolkul, *et al.*, "scikit-hep/iminuit," June, 2023. https://doi.org/10.5281/zenodo.8070217.

[13] T. K. Gaisser, T. Stanev, and S. Tilav *Front. Phys. (Beijing)* **8** (2013) 748–758.

[14] H. P. Dembinski, R. Engel, A. Fedynitch, T. Gaisser, F. Riehn, and T. Stanev *PoS* **ICRC2017** (2018) 533.

Full Author List: IceCube Collaboration

R. Abbasi[17], M. Ackermann[63], J. Adams[18], S. K. Agarwalla[40, 64], J. A. Aguilar[12], M. Ahlers[22], J.M. Alameddine[23], N. M. Amin[44], K. Andeen[42], G. Anton[26], C. Argüelles[14], Y. Ashida[53], S. Athanasiadou[63], S. N. Axani[44], X. Bai[50], A. Balagopal V.[40], M. Baricevic[40], S. W. Barwick[30], V. Basu[40], R. Bay[8], J. J. Beatty[20, 21], J. Becker Tjus[11, 65], J. Beise[61], C. Bellenghi[27], C. Benning[1], S. BenZvi[52], D. Berley[19], E. Bernardini[48], D. Z. Besson[36], E. Blaufuss[19], S. Blot[63], F. Bontempo[31], J. Y. Book[14], C. Boscolo Meneguolo[48], S. Böser[41], O. Botner[61], J. Böttcher[1], E. Bourbeau[22], J. Braun[40], B. Brinson[6], J. Brostean-Kaiser[63], R. T. Burley[2], R. S. Busse[43], D. Butterfield[40], M. A. Campana[49], K. Carloni[14], E. G. Carnie-Bronca[2], S. Chattopadhyay[40, 64], N. Chau[12], C. Chen[6], Z. Chen[55], D. Chirkin[40], S. Choi[56], B. A. Clark[19], L. Classen[43], A. Coleman[61], G. H. Collin[15], A. Connolly[20, 21], J. M. Conrad[15], P. Coppin[13], P. Correa[13], D. F. Cowen[59, 60], P. Dave[6], C. De Clercq[13], J. J. DeLaunay[58], D. Delgado[14], S. Deng[1], K. Deoskar[54], A. Desai[40], P. Desiati[40], K. D. de Vries[13], G. de Wasseige[37], T. DeYoung[24], A. Diaz[15], J. C. Díaz-Vélez[40], M. Dittmer[43], A. Domi[26], H. Dujmovic[40], M. A. DuVernois[40], T. Ehrhardt[41], P. Eller[27], E. Ellinger[62], S. El Mentawi[1], D. Elsässer[23], R. Engel[31, 32], H. Erpenbeck[40], J. Evans[19], P. A. Evenson[44], K. L. Fan[19], K. Fang[40], K. Farrag[16], A. R. Fazely[7], A. Fedynitch[57], N. Feigl[10], S. Fiedlschuster[26], C. Finley[54], L. Fischer[63], D. Fox[59], A. Franckowiak[11], A. Fritz[41], P. Fürst[1], J. Gallagher[39], E. Ganster[1], A. Garcia[14], L. Gerhardt[9], A. Ghadimi[58], C. Glaser[61], T. Glauch[27], T. Glüsenkamp[26, 61], N. Goehlke[32], J. G. Gonzalez[44], S. Goswami[58], D. Grant[24], S. J. Gray[19], O. Gries[1], S. Griffin[40], S. Griswold[52], K. M. Groth[22], C. Günther[1], P. Gutjahr[23], C. Haack[26], A. Hallgren[61], R. Halliday[24], L. Halve[1], F. Halzen[40], H. Hamdaoui[55], M. Ha Minh[27], K. Hanson[40], J. Hardin[15], A. A. Harnisch[24], P. Hatch[33], A. Haungs[31], K. Helbing[62], J. Hellrung[11], F. Henningsen[27], L. Heuermann[1], N. Heyer[61], S. Hickford[62], A. Hidvegi[54], C. Hill[16], G. C. Hill[2], K. D. Hoffman[19], S. Hori[40], K. Hoshina[40, 66], W. Hou[31], T. Huber[31], K. Hultqvist[54], M. Hünnefeld[23], R. Hussain[40], K. Hymon[23], S. In[56], A. Ishihara[16], M. Jacquart[40], O. Janik[1], M. Jansson[54], G. S. Japaridze[5], M. Jeong[56], M. Jin[14], B. J. P. Jones[4], D. Kang[31], W. Kang[56], X. Kang[49], A. Kappes[43], D. Kappesser[41], L. Kardum[23], T. Karg[63], M. Karl[27], A. Karle[40], U. Katz[26], M. Kauer[40], J. L. Kelley[40], A. Khatee Zathul[40], A. Kheirandish[34, 35], J. Kiryluk[55], S. R. Klein[8, 9], A. Kochocki[24], R. Koirala[44], H. Kolanoski[10], T. Kontrimas[27], L. Köpke[41], C. Kopper[26], D. J. Koskinen[22], P. Koundal[31], M. Kovacevich[49], M. Kowalski[10, 63], T. Kozynets[22], J. Krishnamoorthi[40, 64], K. Kruiswijk[37], E. Krupczak[24], A. Kumar[63], E. Kun[11], N. Kurahashi[49], N. Lad[63], C. Lagunas Gualda[63], M. Lamoureux[37], M. J. Larson[19], S. Latseva[1], F. Lauber[62], J. P. Lazar[14, 40], J. W. Lee[56], K. Leonard DeHolton[60], A. Leszczyńska[44], M. Lincetto[11], Q. R. Liu[40], M. Liubarska[25], E. Lohfink[41], C. Love[49], C. J. Lozano Mariscal[43], L. Lu[40], F. Lucarelli[28], W. Luszczak[20, 21], Y. Lyu[8, 9], J. Madsen[40], K. B. M. Mahn[24], Y. Makino[40], E. Manao[27], S. Mancina[40, 48], W. Marie Sainte[40], I. C. Mariş[12], S. Marka[46], Z. Marka[46], M. Marsee[58], I. Martinez-Soler[14], R. Maruyama[45], F. Mayhew[24], T. McElroy[25], F. McNally[38], J. V. Mead[22], K. Meagher[40], S. Mechbal[63], A. Medina[21], M. Meier[16], Y. Merckx[13], L. Merten[11], J. Micallef[24], J. Mitchell[7], T. Montaruli[28], R. W. Moore[25], Y. Morii[16], R. Morse[40], M. Moulai[40], T. Mukherjee[31], R. Naab[63], R. Nagai[16], M. Nakos[40], U. Naumann[62], J. Necker[63], A. Negi[4], M. Neumann[43], H. Niederhausen[24], M. U. Nisa[24], A. Noell[1], A. Novikov[44], S. C. Nowicki[24], A. Obertacke Pollmann[16], V. O'Dell[40], M. Oehler[31], B. Oeyen[29], A. Olivas[19], R. Ørsøe[27], J. Osborn[40], E. O'Sullivan[61], H. Pandya[44], N. Park[33], G. K. Parker[4], E. N. Paudel[44], L. Paul[42, 50], C. Pérez de los Heros[61], J. Peterson[40], S. Philippen[1], A. Pizzuto[40], M. Plum[50], A. Pontén[61], Y. Popovych[41], M. Prado Rodriguez[40], B. Pries[24], R. Procter-Murphy[19], G. T. Przybylski[9], C. Raab[37], J. Rack-Helleis[41], K. Rawlins[3], Z. Rechav[40], A. Rehman[44], P. Reichherzer[11], G. Renzi[12], E. Resconi[27], S. Reusch[63], W. Rhode[23], B. Riedel[40], A. Rifaie[1], E. J. Roberts[2], S. Robertson[8, 9], S. Rodan[56], G. Roellinghoff[56], M. Rongen[26], C. Rott[53, 56], T. Ruhe[23], L. Ruohan[27], D. Ryckbosch[29], I. Safa[14, 40], J. Saffer[32], D. Salazar-Gallegos[24], P. Sampathkumar[31], S. E. Sanchez Herrera[24], A. Sandrock[62], M. Santander[58], S. Sarkar[25], S. Sarkar[47], J. Savelberg[1], P. Savina[40], M. Schaufel[1], H. Schieler[31], S. Schindler[26], L. Schlickmann[1], B. Schlüter[43], F. Schlüter[12], N. Schmeisser[62], T. Schmidt[19], J. Schneider[26], F. G. Schröder[31, 44], L. Schumacher[26], G. Schwefer[1], S. Sclafani[19], D. Seckel[44], M. Seikh[36], S. Seunarine[51], R. Shah[49], A. Sharma[61], S. Shefali[32], N. Shimizu[16], M. Silva[40], B. Skrzypek[14], B. Smithers[4], R. Snihur[40], J. Soedingrekso[23], A. Søgaard[22], D. Soldin[32], P. Soldin[1], G. Sommani[11], C. Spannfellner[27], G. M. Spiczak[51], C. Spiering[63], M. Stamatikos[21], T. Stanev[44], T. Stezelberger[9], T. Stürwald[62], T. Stuttard[22], G. W. Sullivan[19], I. Taboada[6], S. Ter-Antonyan[7], M. Thiesmeyer[1], W. G. Thompson[14], J. Thwaites[40], S. Tilav[44], K. Tollefson[24], C. Tönnis[56], S. Toscano[12], D. Tosi[40], A. Trettin[63], C. F. Tung[6], R. Turcotte[31], J. P. Twagirayezu[24], B. Ty[40], M. A. Unland Elorrieta[43], A. K. Upadhyay[40, 64], K. Upshaw[7], N. Valtonen-Mattila[61], J. Vandenbroucke[40], N. van Eijndhoven[13], D. Vannerom[15], J. van Santen[63], J. Vara[43], J. Veitch-Michaelis[40], M. Venugopal[31], M. Vereecken[37], S. Verpoest[44], D. Veske[46], A. Vijai[19], C. Walck[54], C. Weaver[24], P. Weigel[15], A. Weindl[31], J. Weldert[60], C. Wendt[40], J. Werthebach[23], M. Weyrauch[31], N. Whitehorn[24], C. H. Wiebusch[1], N. Willey[24], D. R. Williams[58], L. Witthaus[23], A. Wolf[1], M. Wolf[27], G. Wrede[26], X. W. Xu[7], J. P. Yanez[25], E. Yildizci[40], S. Yoshida[16], R. Young[36], F. Yu[14], S. Yu[24], T. Yuan[40], Z. Zhang[55], P. Zhelnin[14], M. Zimmerman[40]

[1] III. Physikalisches Institut, RWTH Aachen University, D-52056 Aachen, Germany
[2] Department of Physics, University of Adelaide, Adelaide, 5005, Australia
[3] Dept. of Physics and Astronomy, University of Alaska Anchorage, 3211 Providence Dr., Anchorage, AK 99508, USA
[4] Dept. of Physics, University of Texas at Arlington, 502 Yates St., Science Hall Rm 108, Box 19059, Arlington, TX 76019, USA
[5] CTSPS, Clark-Atlanta University, Atlanta, GA 30314, USA
[6] School of Physics and Center for Relativistic Astrophysics, Georgia Institute of Technology, Atlanta, GA 30332, USA
[7] Dept. of Physics, Southern University, Baton Rouge, LA 70813, USA
[8] Dept. of Physics, University of California, Berkeley, CA 94720, USA
[9] Lawrence Berkeley National Laboratory, Berkeley, CA 94720, USA
[10] Institut für Physik, Humboldt-Universität zu Berlin, D-12489 Berlin, Germany
[11] Fakultät für Physik & Astronomie, Ruhr-Universität Bochum, D-44780 Bochum, Germany
[12] Université Libre de Bruxelles, Science Faculty CP230, B-1050 Brussels, Belgium

[13] Vrije Universiteit Brussel (VUB), Dienst ELEM, B-1050 Brussels, Belgium
[14] Department of Physics and Laboratory for Particle Physics and Cosmology, Harvard University, Cambridge, MA 02138, USA
[15] Dept. of Physics, Massachusetts Institute of Technology, Cambridge, MA 02139, USA
[16] Dept. of Physics and The International Center for Hadron Astrophysics, Chiba University, Chiba 263-8522, Japan
[17] Department of Physics, Loyola University Chicago, Chicago, IL 60660, USA
[18] Dept. of Physics and Astronomy, University of Canterbury, Private Bag 4800, Christchurch, New Zealand
[19] Dept. of Physics, University of Maryland, College Park, MD 20742, USA
[20] Dept. of Astronomy, Ohio State University, Columbus, OH 43210, USA
[21] Dept. of Physics and Center for Cosmology and Astro-Particle Physics, Ohio State University, Columbus, OH 43210, USA
[22] Niels Bohr Institute, University of Copenhagen, DK-2100 Copenhagen, Denmark
[23] Dept. of Physics, TU Dortmund University, D-44221 Dortmund, Germany
[24] Dept. of Physics and Astronomy, Michigan State University, East Lansing, MI 48824, USA
[25] Dept. of Physics, University of Alberta, Edmonton, Alberta, Canada T6G 2E1
[26] Erlangen Centre for Astroparticle Physics, Friedrich-Alexander-Universität Erlangen-Nürnberg, D-91058 Erlangen, Germany
[27] Technical University of Munich, TUM School of Natural Sciences, Department of Physics, D-85748 Garching bei München, Germany
[28] Département de physique nucléaire et corpusculaire, Université de Genève, CH-1211 Genève, Switzerland
[29] Dept. of Physics and Astronomy, University of Gent, B-9000 Gent, Belgium
[30] Dept. of Physics and Astronomy, University of California, Irvine, CA 92697, USA
[31] Karlsruhe Institute of Technology, Institute for Astroparticle Physics, D-76021 Karlsruhe, Germany
[32] Karlsruhe Institute of Technology, Institute of Experimental Particle Physics, D-76021 Karlsruhe, Germany
[33] Dept. of Physics, Engineering Physics, and Astronomy, Queen's University, Kingston, ON K7L 3N6, Canada
[34] Department of Physics & Astronomy, University of Nevada, Las Vegas, NV, 89154, USA
[35] Nevada Center for Astrophysics, University of Nevada, Las Vegas, NV 89154, USA
[36] Dept. of Physics and Astronomy, University of Kansas, Lawrence, KS 66045, USA
[37] Centre for Cosmology, Particle Physics and Phenomenology - CP3, Université catholique de Louvain, Louvain-la-Neuve, Belgium
[38] Department of Physics, Mercer University, Macon, GA 31207-0001, USA
[39] Dept. of Astronomy, University of Wisconsin–Madison, Madison, WI 53706, USA
[40] Dept. of Physics and Wisconsin IceCube Particle Astrophysics Center, University of Wisconsin–Madison, Madison, WI 53706, USA
[41] Institute of Physics, University of Mainz, Staudinger Weg 7, D-55099 Mainz, Germany
[42] Department of Physics, Marquette University, Milwaukee, WI, 53201, USA
[43] Institut für Kernphysik, Westfälische Wilhelms-Universität Münster, D-48149 Münster, Germany
[44] Bartol Research Institute and Dept. of Physics and Astronomy, University of Delaware, Newark, DE 19716, USA
[45] Dept. of Physics, Yale University, New Haven, CT 06520, USA
[46] Columbia Astrophysics and Nevis Laboratories, Columbia University, New York, NY 10027, USA
[47] Dept. of Physics, University of Oxford, Parks Road, Oxford OX1 3PU, United Kingdom
[48] Dipartimento di Fisica e Astronomia Galileo Galilei, Università Degli Studi di Padova, 35122 Padova PD, Italy
[49] Dept. of Physics, Drexel University, 3141 Chestnut Street, Philadelphia, PA 19104, USA
[50] Physics Department, South Dakota School of Mines and Technology, Rapid City, SD 57701, USA
[51] Dept. of Physics, University of Wisconsin, River Falls, WI 54022, USA
[52] Dept. of Physics and Astronomy, University of Rochester, Rochester, NY 14627, USA
[53] Department of Physics and Astronomy, University of Utah, Salt Lake City, UT 84112, USA
[54] Oskar Klein Centre and Dept. of Physics, Stockholm University, SE-10691 Stockholm, Sweden
[55] Dept. of Physics and Astronomy, Stony Brook University, Stony Brook, NY 11794-3800, USA
[56] Dept. of Physics, Sungkyunkwan University, Suwon 16419, Korea
[57] Institute of Physics, Academia Sinica, Taipei, 11529, Taiwan
[58] Dept. of Physics and Astronomy, University of Alabama, Tuscaloosa, AL 35487, USA
[59] Dept. of Astronomy and Astrophysics, Pennsylvania State University, University Park, PA 16802, USA
[60] Dept. of Physics, Pennsylvania State University, University Park, PA 16802, USA
[61] Dept. of Physics and Astronomy, Uppsala University, Box 516, S-75120 Uppsala, Sweden
[62] Dept. of Physics, University of Wuppertal, D-42119 Wuppertal, Germany
[63] Deutsches Elektronen-Synchrotron DESY, Platanenallee 6, 15738 Zeuthen, Germany
[64] Institute of Physics, Sachivalaya Marg, Sainik School Post, Bhubaneswar 751005, India
[65] Department of Space, Earth and Environment, Chalmers University of Technology, 412 96 Gothenburg, Sweden
[66] Earthquake Research Institute, University of Tokyo, Bunkyo, Tokyo 113-0032, Japan

Acknowledgements

The authors gratefully acknowledge the support from the following agencies and institutions: USA – U.S. National Science Foundation-Office of Polar Programs, U.S. National Science Foundation-Physics Division, U.S. National Science Foundation-EPSCoR, Wisconsin Alumni Research Foundation, Center for High Throughput Computing (CHTC) at the University of Wisconsin–Madison, Open Science

Grid (OSG), Advanced Cyberinfrastructure Coordination Ecosystem: Services & Support (ACCESS), Frontera computing project at the Texas Advanced Computing Center, U.S. Department of Energy-National Energy Research Scientific Computing Center, Particle astrophysics research computing center at the University of Maryland, Institute for Cyber-Enabled Research at Michigan State University, and Astroparticle physics computational facility at Marquette University; Belgium – Funds for Scientific Research (FRS-FNRS and FWO), FWO Odysseus and Big Science programmes, and Belgian Federal Science Policy Office (Belspo); Germany – Bundesministerium für Bildung und Forschung (BMBF), Deutsche Forschungsgemeinschaft (DFG), Helmholtz Alliance for Astroparticle Physics (HAP), Initiative and Networking Fund of the Helmholtz Association, Deutsches Elektronen Synchrotron (DESY), and High Performance Computing cluster of the RWTH Aachen; Sweden – Swedish Research Council, Swedish Polar Research Secretariat, Swedish National Infrastructure for Computing (SNIC), and Knut and Alice Wallenberg Foundation; European Union – EGI Advanced Computing for research; Australia – Australian Research Council; Canada – Natural Sciences and Engineering Research Council of Canada, Calcul Québec, Compute Ontario, Canada Foundation for Innovation, WestGrid, and Compute Canada; Denmark – Villum Fonden, Carlsberg Foundation, and European Commission; New Zealand – Marsden Fund; Japan – Japan Society for Promotion of Science (JSPS) and Institute for Global Prominent Research (IGPR) of Chiba University; Korea – National Research Foundation of Korea (NRF); Switzerland – Swiss National Science Foundation (SNSF); United Kingdom – Department of Physics, University of Oxford.